HAL
open science

Ligand-free synthesis of gold nanoparticles incorporated within cylindrical block copolymer films

Florian Aubrit, Testard Fabienne, Aurélie Paquirissamy, Frédéric Gobeaux, Xuan Wang, Frédéric Nallet, Philippe Fontaine, Virginie Ponsinet, Patrick Guenoun

To cite this version:

Florian Aubrit, Testard Fabienne, Aurélie Paquirissamy, Frédéric Gobeaux, Xuan Wang, et al.. Ligand-free synthesis of gold nanoparticles incorporated within cylindrical block copolymer films. Journal of Materials Chemistry C, inPress, 6 (30), pp.8194-8204. 10.1039/C8TC01477A . cea-01839711

HAL Id: cea-01839711

https://cea.hal.science/cea-01839711

Submitted on 16 Jul 2018

HAL is a multi-disciplinary open access archive for the deposit and dissemination of scientific research documents, whether they are published or not. The documents may come from teaching and research institutions in France or abroad, or from public or private research centers.

L'archive ouverte pluridisciplinaire **HAL**, est destinée au dépôt et à la diffusion de documents scientifiques de niveau recherche, publiés ou non, émanant des établissements d'enseignement et de recherche français ou étrangers, des laboratoires publics ou privés.

Published on 10 July 2018. Downloaded on 7/16/2018 5:59:18 AM.

Ligand-free synthesis of gold nanoparticles included within cylindrical block copolymer films

Florian Aubrit,[a,b] Fabienne Testard,[a] Aurélie Paquirissamy,[a] Frédéric Gobeaux,[a] Xuan Wang,[b] Frédéric Nallet,[b] Philippe Fontaine,[c] Virginie Ponsinet*[b] and Patrick Guenoun[a]

We report a method to include non-functionalized gold nanoparticles (AuNPs) in oriented cylindrical phases of poly(styrene)-b-poly(vinylpyridine) (PS-b-PVP) block copolymers, perpendicular or parallel to a substrate. The combination of AFM, TEM, GISAXS and spectroscopy allows a complete characterization of the nanocomposite. AuNPs are produced by the ultra-sound reduction of a gold salt in the copolymer solution, prior to the deposition of the film by spin-coating. The AuNPs are found to be located within the PVP cylinders exclusively. Sizes from 2 to 4 nm are tuned as a function of the initial gold salt concentration. A seeded-growth of these pre-formed AuNPs was also achieved by a further ultra-sound treatment to produce larger AuNPs (up to d=10 nm) with plasmon resonance properties. For parallel cylinders, the presence of AuNPs in the PVP domains disturbs the organization, while, for perpendicular cylinders, the PVP domains are swollen without any change in their orientation. The synthesis of AuNPs inside the copolymer was also performed by radiolysis, through the irradiation of the copolymer solution or the copolymer film, both containing the gold salt. In these cases, the presence of plasmonic AuNPs was also evidenced. Offering a control of the AuNPs size (< 2 nm to 10 nm) and location, the presented method is a promising way of inserting plasmonic AuNPs into oriented cylinders for reaching anisotropic geometries of valuable interest for optics.

Introduction

Hybrid nanocomposites including noble metal nanostructures have become of great interest for their unique optical, electrical, and mechanical properties[1,2]. They are essential elements of nanophotonics which explore the possibility of modulating light propagation with very small amount of matter using nanoscale phenomena. The occurrence of plasmons at metal/dielectric interfaces is indeed one of the key phenomena used in nanophotonics, which has encouraged in the recent years active research towards the fabrication of nanostructured noble metal-dielectric materials and surfaces. In this context, an increasing interest focuses on the incorporation of gold nanoparticles (AuNPs) into block copolymer (BCP) matrices, which allows the combination of the specific physical properties of the AuNPs –their localized surface plasmon resonance[3,4] – with the ability of the BCP to self-assemble into well-organized 3D nanostructures[5,6,7,8], such as assemblies of lamellae, cylinders or spheres. Such materials, patterned at the nanometer scale can provide bricks to a wide range of applications in optics[9,10,11,12,13] and electronics[14,15]. Particularly, block copolymers provide anisotropic templates of interest for reaching unusual light propagation properties such as the one of the so-called "hyperbolic metamaterials", with several promising applications[16,17].

The last few years have seen the development of various methodologies to incorporate nanoparticles in self-assembled block copolymer matrices[18,19]. The majority of the studies focused so far on lamellar nanostructures, but oriented cylinders could provide a stronger confinement of AuNPs and offer different optical anisotropies than lamellae. However, very few methods to include AuNPs in such cylinders embedded in copolymer films have been reported so far[20,21]. Note that, on the opposite, quite a few studies have made use of such cylinders or other block copolymer morphologies as templates to produce 2D arrays of nanoparticles[22,23,24,25,26].

In the case of insertion within lamellae, two main paths have been developed. The nanoparticles can be either pre-formed and then inserted inside the polymer matrix (often called *ex situ* method), or be synthetized *in situ* through the selective reduction of metal ion in one of the block domains. The first method often uses nanoparticles functionalized with a ligand compatible with the polymer block in which they are to be inserted: for instance, in the case of a matrix of poly(styrene)-b-poly(vinylpyridine) (PS-b-PVP) presenting spheres of PVP, insertion has been achieved through the functionalization with

[a.] *Laboratoire Interdisciplinaire sur l'Organisation Nanométrique et Supramoléculaire (LIONS), NIMBE, CEA, CNRS, Université Paris-Saclay, CEA-Saclay 91191 Gif-sur-Yvette Cedex (France).*
[b.] *Univ. Bordeaux, CNRS, Centre de Recherche Paul Pascal (CRPP), UMR 5031, 33600 Pessac (France). *Email - ponsinet@crpp-bordeaux.cnrs.fr*
[c.] *Synchrotron SOLEIL, L'Orme des Merisiers, Saint-Aubin-BP 48, F-91192 Gif-sur Yvette Cedex (France).*
Electronic Supplementary Information (ESI) available: [GISAXS model description and Figures S1 to S7]. See DOI: 10.1039/x0xx00000x

thiol-PVP[27] or pyridine[28] ligands. This method allows a good control on the shape and size of the nanoparticles[21,29]

However, the insertion of large quantities of such nanoparticles within block copolymer mesophases can be difficult to achieve, because of steric hindrance, especially for particles of large dimensions[30]. This issue can be tackled by the second method of *in situ* formation of the nanoparticles. Gold nanoparticles can be generated by successive cycles of liquid chemical permeation of a gold salt followed by a reducing agent[11,31]. However, because of the increased confinement of cylindrical structures as compared to lamellae, it can be difficult to find the right balance between –i- an insufficient swelling of the matrix, leading to incomplete diffusion of the precursor reagents and therefore gradients in the filler concentration[32], and –ii- a too efficient swelling leading to structure disruption. In particular, the immersion in aqueous or ethanolic solutions –containing the gold salt and/or the reducing agent– can damage the film structure due to nanodomain swelling[33]. Because there is still a need for simple strategies able to build a nanocomposite made from perpendicular cylinders full of AuNPs, we considered here an alternative strategy consisting in the direct synthesis of the AuNPs in the copolymer solution prior to the film formation. We made use of physico-chemical methods such as γ-irradiation[34,35,36] or sonication[37,38,39] for the reduction of gold salt in aqueous solutions, with no need for the addition of a reducing agent. Only few results have appeared, so far, about producing gold nanoparticles by irradiation or sonication directly in organic media. The study of Surendran *et al.* on the formation of platinum nanoparticles in liquid crystal by radiolysis[40] is close to our approach, but no process of NPs formation by sonication in a copolymer solution to form a nanostructured films was reported to our knowledge.

Here, we report on the formation of PS-b-PVP films organized in cylindrical mesophases and containing AuNPs. First, the full characterization of the perpendicular or parallel cylinders of PS-b-P4VP and PS-b-P2VP was achieved with Atomic Force Microscopy (AFM), Transmission Electronic Microscopy (TEM) and Grazing-Incidence Small-Angle X-ray Scattering (GISAXS) experiments. Then, the incorporation of AuNPs was obtained by a two steps procedure: 1/ the AuNPs were produced directly by sonication of the solution prior to 2/ the casting of the film. This synthesis method avoids adding extra-species such as a ligand or reducing agent in the solution. We also proved the efficiency of a seeded-growth method to reach larger AuNPs exhibiting a plasmon resonance.

The AuNPs formation was also achieved by radiolysis in solution before casting, as well as directly on the previously deposited film, both leading to films containing AuNPs of small diameter located into the cylinders and exhibiting a plasmon resonance. These processes of sonication, or irradiation, and spin-coating of a gold-containing copolymer solution allow for an easy and controllable formation of self-organized plasmonic hybrid films.

A first optical characterization of these films was achieved by variable angle spectroscopic ellipsometry. In particular, a p-polarized visible radiation incident on the films containing the plasmonic nanoparticles presents an extinction accompanied by a phase jump at a specific wavelength and incidence angle. Furthermore, these wavelengths and angles were found to depend on the nanoparticle size.

Experimental section

Materials.

Two different diblock copolymers of poly(styrene)-block-poly(4-vinylpyridine) (PS-b-P4VP) and one diblock copolymer of poly(styrene)-block-poly(2-vinylpyridine) (PS-b-P2VP), of formula $(C_8H_8)_n$-b-$(C_7H_7N)_m$, were purchased from Polymer Source, Inc., and used as received. Table 1 summarized the composition of the three different polymers. In this report, these polymers will be referred to as PS_x-b-PVP_y with x and y the molecular mass of each block, respectively, in kg/mol.

Gold (III) chloride ($AuCl_3$, 99,99%) and sodium bromide (NaBr) were purchased from Sigma Aldrich and used as received.

Substrate preparation.

Silicon (Si) substrates of 1 cm^2 were cleaned by immersion for 2 hours in a mixture of deionized water/hydrogen peroxide (H_2O_2)/ammonia (NH_3) (5:1:1) before conservation in a Petri dish. Before any utilization, the wafers were exposed to a plasma (created from ionized dioxygen) at low pressure during 3 min, for a thorough cleaning. For glass substrates, microscope glass slides (with a thickness of 3 mm) were cut into pieces of 1 cm^2. Those pieces were treated by the same plasma cleaning for 3 min before utilization.

Films preparation.

Perpendicular cylinders. The PS_{48}-b-$P4VP_{25}$ and PS_{27}-b-$P4VP_7$ copolymers were dissolved in a mixture of toluene/tetrahydrofurane (THF) (with various ratio according to the nature of the copolymer, for details see Table 1) in order to yield 1 wt% solutions. These solutions were spin-cast at 2000 rpm for 1 minute to yield ≈ 100 nm-thick films. The residual solvent in the spin-cast films was removed by placing the films in vacuum for 2 h. For some samples, a solvent annealing in vapors of a mixture chloroform/ethanol ($CHCl_3$/EtOH) (10:1) was performed for 1 min at 60°C. The films were then quickly removed from the vapor chamber and dried with nitrogen and finally placed in vacuum for 2 h.

Parallel cylinders. The PS_{34}-b-$P2VP_{18}$ copolymer was dissolved in $CHCl_3$ in order to yield a 0.5 wt% solution. This solution was spin-cast at 2000 rpm for 1 minute to yield ≈ 100 nm-thick films, then dried with nitrogen. A solvent annealing in $CHCl_3$ vapors was performed for 1 min at 60°C. The films were then dried again with nitrogen and placed in vacuum for 2 h.

Published on 10 July 2018. Downloaded on 7/16/2018 5:59:18 AM.

Name	Copolymer	M_n(PS) (g.mol^{-1})	M_n(PVP) (g.mol^{-1})	M_n/M_w	Solvent
PS_{27}-b-$P4VP_7$	P8372-S4VP	27,000	7,000	1.15	Toluene/THF (80 :20)
PS_{48}-b-$P4VP_{25}$	P11258-S4VP	48,000	25,000	1.15	Toluene/THF (90 :10)
PS_{34}-b-$P2VP_{18}$	P8404-S2VP	34,000	18,000	1.12	Chloroform

Table 1. Properties of the copolymers used. M_n/M_w is the polydispersity index of the polymer.

***In situ* formation of the gold nanoparticles (AuNPs) by sonication.**

Copolymer solutions were prepared as described above, then mixed with a 0.1 M $AuCl_3$ solution in toluene (in chloroform for parallel cylinders) in order to obtain various gold/pyridine molar ratios (from Au/pyr = 0.1 to Au/pyr = 5.5). The solution was protected from light and stirred overnight. The AuNPs were synthetized by sonication as follows: the solution vial was immersed in the sonication bath (Elmasonic P30H, 37 kHz, 120 W) and sonicated for a given time (from 1 to 10 min) at room temperature. A film was then spin-cast as described above.
Seeded growth kinetics were performed by adding gold salt (Au/pyr = 0.2, each addition) in the copolymer solution containing the previously formed AuNPs (initially with a ratio Au/pyr = 0.5). The mixture was sonicated again to grow metallic gold on the surface of the AuNPs. This process of gold addition/sonication was repeated three times, in order to get AuNPs bigger in size.

***In situ* formation of the gold nanoparticles (AuNPs) by radiolysis.**

Copolymer solutions were prepared as described, then mixed with a 0.03 M $AuCl_3$ solution in toluene in order to obtain a solution with a ratio Au/pyr = 0.5. The solution was stirred for 1 hour, away from any light. A film was obtained by spin-coating some of the solution on a glass slide as described above.
Both solution and film were then irradiated with a Gammacell (300 Elan) equipped with a Cesium 137 source with energy 660 keV. The dose rate used was 5.6 Gy/min, as determined by Fricke dosimetry. For both approaches, the kinetics of the formation were studied ex situ (with UV-visible spectroscopy) by varying the irradiation time from 1h to 24h (0.33 to 8 kGy). Such a dose range is expected to have minimal damaging effects on aromatic polymers like the one used here.

Characterization.

Atomic Force Microscopy (AFM) measurements were carried out with a Bruker-NanoDimension 3000 AFM equipped with a Nanoscope V controller in tapping mode using NanoWorld ARROW-NCR silicon cantilevers (f_0 = 240 - 380 kHz, k = 27 – 80 N/m, as specified by the manufacturer). AFM images were typically obtained with scan ranges of 3 x 3 µm^2, 1 x 1 µm^2 and 300 x 300 nm^2 at a frequency of 0.8 line/second. Film thicknesses were measured by scratching the film on the whole length with a razor blade followed by scanning across the scratch edges.
Transmission Electron Microscopy (TEM) measurements were performed on a CM30 transmission electron microscope operating at an accelerating voltage of 300 kV. The mixed polymer/AuNPs suspensions were drop-cast on a carbonated copper grid and let evaporate overnight before analysis. There was no addition of contrast agent before the TEM observation.
UV-visible spectroscopy was carried out on a UV-2550 Shimadzu spectroscope in a wavelength range from 190 to 900 nm. For the study of the mixed polymer/AuNPs suspensions, the signal obtained with a neat copolymer solution in the same cell was subtracted in order to extract the signal of the gold species (salt and NPs). For the study of the films deposited and γ-irradiated on glass slides, we subtracted the signal measured on a reference glass slide after irradiation, since glass evolves while irradiated.
GISAXS experiments were performed on the SIRIUS beamline[41] of SOLEIL synchrotron (Gif-sur-Yvette, FRANCE). The configuration was obtained with a 2D Pilatus3 (Dectris Ltd, Switzerland) detector positioned at 4.45 meters from the samples allowing for one single distance acquisition for all the samples. A vertical beamstop is mounted to catch the vertical specular and off-specular reflection from the surface. The energy of the incident X-Ray beam was fixed at 7.8 keV and the beamsize was 100×500 µm^2 (vertical×horizontal). Various incidence angles (from 2 mrad to 4 mrad) were measured starting from below the critical angle of the silicon substrate (4.02 mrad). Data were fitted with a monodisperse 2D-hexagonal model, with the help of the FitGISAXS software elaborated by D. Babonneau[42] (see Supp. Info for detail).
The optical study was performed using **variable angle spectroscopic ellipsometry** (VASE) in reflection with a phase modulated spectroscopic ellipsometer (UVISEL, from Horiba Scientific) on the spectral range [275-2000 nm or alternatively 0.6-4.5 eV]. We used the UVISEL II (A=45°; M=0) configuration, where A and M denote the azimuthal orientations of the input polarizer and photoelastic modulator, respectively, with respect to the plane of incidence. Five values of the incidence angle θ_0=50°, 55°, 60°, 65° and 70° were used and analyzed simultaneously. The spot size was 1 mm and the measured data were checked to be similar at three different locations on the samples. We acquired the ellipsometric quantities $I_s=\sin^2(\Psi)\sin(\Delta)$ and $I_c=\sin^2(\Psi)\cos(\Delta)$, where Ψ and Δ are the two ellipsometric angles, defined by the ellipsometric ratio $\rho=r_p/r_s=\tan(\Psi).e^{i\Delta}$, with r_p and r_s the complex reflection coefficients of the amplitude of the p-polarized (*i.e.* in the plane of incidence) and the s-polarized (perpendicular to the

Published on 10 July 2018. Downloaded on 7/16/2018 5:59:18 AM.

Published on 10 July 2018. Downloaded on 7/16/2018 5:59:18 AM.

plane of incidence) waves respectively. We also represent the experimental data as the value of the pseudo-dielectric function:

$$\tilde{\varepsilon} = \tilde{\varepsilon}_r + i.\tilde{\varepsilon}_i = sin^2(\theta_0)\left[1 + \left(\frac{1-\rho}{1+\rho}\right)^2 tan^2(\theta_0)\right],$$

which corresponds to the dielectric function of a hypothetical bulk material providing the same ellipsometric measurements as the studied thin film. The VASE information was obtained by measuring the full spectra for the films at different growth steps of the gold nanoparticles.

Results and discussion

Organization of the block copolymer film.

Two types of PS-b-P4VP (see Table 1) were used to produce spin-cast films (with a thickness typically 100 nm) presenting arrays of cylinders normal to the substrate. In order to obtain a perpendicular orientation of the cylinders, the copolymer was dissolved in a dedicated solvent – a mixture toluene/THF, with a ratio depending on the molecular mass of each block – as described in the literature[43]. Figure 1 shows AFM height images of a PS_{27}-b-$P4VP_7$ with a 2D-hexagonal organization of perpendicular cylinders. The spin-coating process with the chosen solvent is able to orient the cylinders normal to the surface, on various substrates like glass slide or silicon wafers, suggesting that the surface energy has no effect and that a metastable state is reached: the final perpendicular organization disappears when energy is provided, such as during a thermal annealing of the film. From the AFM images, in which the contrast comes from a slight height difference between two block domains, the structural parameters such as the cylinder center-to-center distance and cylinder diameter can be estimated. The Table 2 summarizes the average values obtained for the different samples, depending on their composition and concentration before spin-coating. The spin-coating parameters were the same for all the samples presented in this table.

Sample	wt %	D (nm)	Λ (nm)	H (nm)
PS_{27}-b-$P4VP_7$	1	25	45	85
PS_{27}-b-$P4VP_7$	3	24	37	100
PS_{48}-b-$P4VP_{25}$	1.5	35	65	160
PS_{48}-b-$P4VP_{25}$	2	32	63	270

Table 2. AFM-extracted structural parameters of the block copolymer films: D is the diameter of the cylinders, Λ is the center-to-center distance between two neighboring cylinders, and H is the thickness of the film. These parameters depends on the molecular weight of each block of the copolymers and on the weight concentration (wt%) of the copolymer in solution.

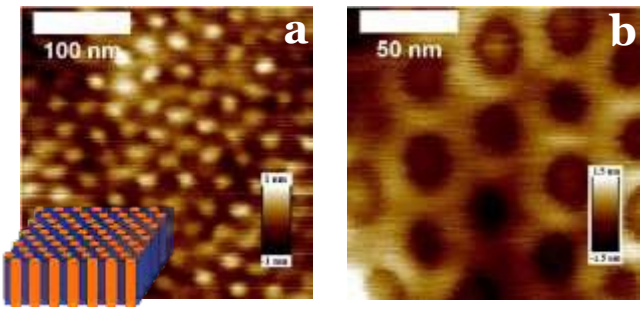

Figure 1. a/ AFM height image of a PS27-b-P4VP7 film oriented in perpendicular cylinders, with a schematic of the film 3D organization; b/ AFM height image of the same sample after annealing in vapors of $CHCl_3$:EtOH (10:1), showing a phase separation with higher contrast and inverted topography.

The influence of the solvent annealing is visible on the upper surface of the PVP cylinders: while the cylinders are higher than the PS matrix before annealing, they become lower with the annealing procedure (Figure 1), due to the matrix expansion after the solvent exposition.

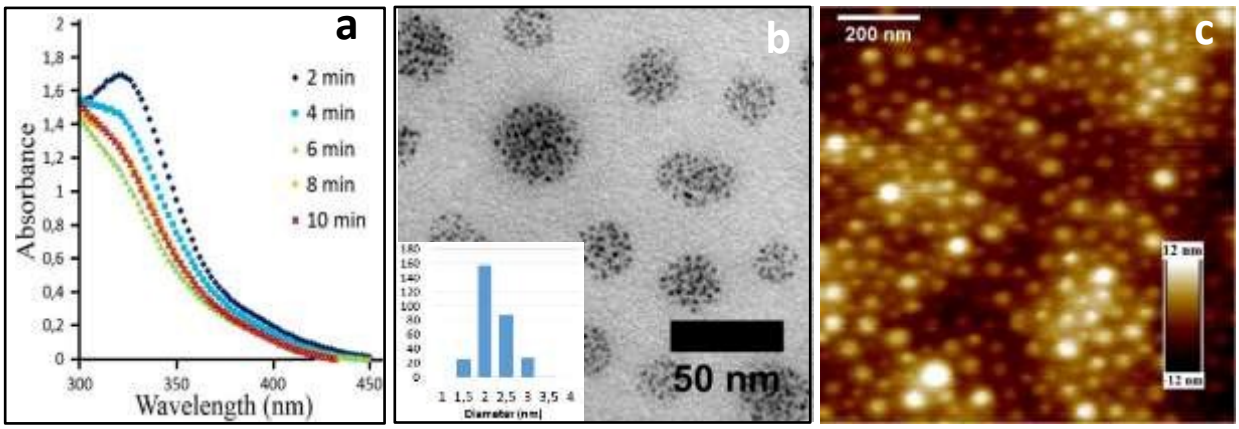

Figure 3. a/ UV-visible spectra (without the contribution of the copolymer) showing the decrease of the characteristic peak for Au(III) over time; b/ TEM picture of the AuNPs confined in the PVP domain of PS_{27}-b-$P4VP_7$, with inset the size distribution of the AuNP diameter over 300 particles. The average diameter is around 2 nm; c/ the equivalent AFM height picture showing the cylinder organization in surface. The ratio gold/pyridine for this sample was 0.5.

Published on 10 July 2018. Downloaded on 7/16/2018 5:59:18 AM.

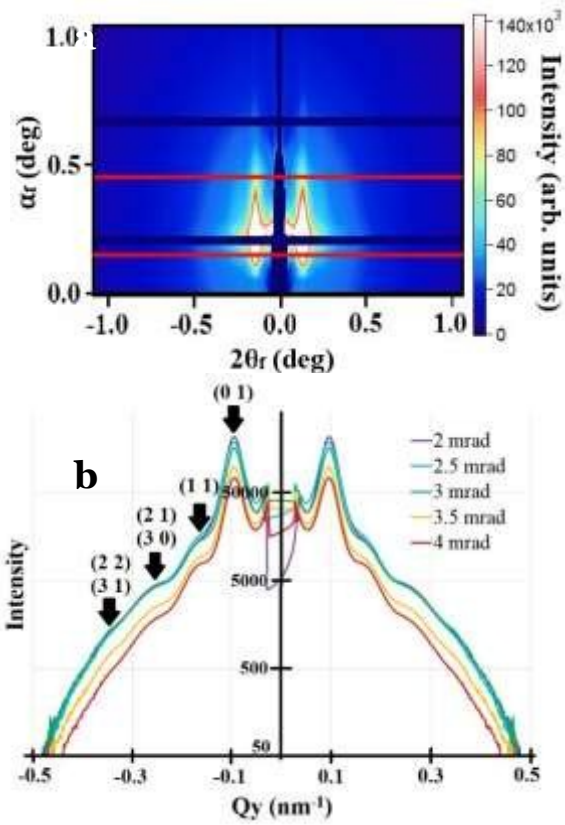

Figure 2. a/ GISAXS pattern of a PS_{48}-b-$P4VP_{25}$ film for an incidence angle of 3 mrad and the corresponding intensity versus Q_y curve (integrated between the two red lines of a)) with b/ intensity versus Q_y curves for all the incidence angles analyzed, after fitting and removal of the Gaussian-shaped background. The black arrows point out the structural peaks, corresponding to a hexagonal lattice.

The persistence of the morphology through the whole film thickness was investigated by Grazing-Incidence Small-Angle X-ray Scattering (GISAXS). The 2D patterns (Figure 2.a) present typical features of an ordered film. Integration of the scattered intensity for $0.20<Q_z<0.50$ nm^{-1} yields a function $I(Q_y)$ giving access to the in-plane organization in the films.

After removing a Gaussian-shaped background originating from the polymer matrix and independently measured (see Supp. Info), the resulting data present several peaks (shown with black arrows on Figure 2.b), in accordance with the different orders of a 2D hexagonal packing. Several incidence angles (from 2 mrad to 4 mrad) were analyzed to determine the geometry of the films for different penetration depths. For the different angles, the first order is well defined, as well as the second and third orders; the fourth order is less visible. A first conclusion is that the microphase separation is present all over the thickness of the film although with a slighty increasing disorder with depth. The position of the first peak gives information about the distance between the centers of two neighboring cylinders. The GISAXS curve after removal of the background at 3 mrad and the Fast Fourier Transform (FFT) from a AFM height image of a PS_{48}-b-$P4VP_{25}$ film surface (shown in sup. info.; S4) were compared to check the

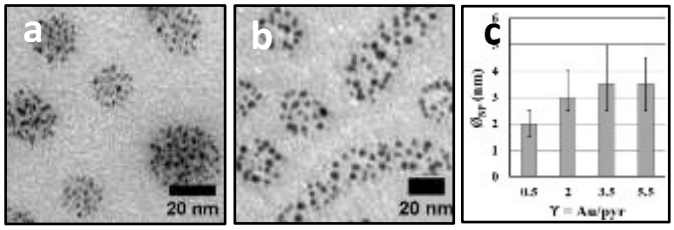

Figure 4. TEM pictures of the PVP domain of PS27-b-P4VP7 containing AuNPs formed by sonication for an initial ratio gold/pyridine of a/ 0.5 and b/ 5.5, and c/ evolution of the nanoparticle diameter with the ratio gold/pyridine.

consistency of both methods. The position of the first peak from both methods leads to an identical value $q_{(01)} = 0.1$ nm^{-1}, corresponding to a cylinder center-to-center distance $\Lambda = 60$ nm. The higher order peaks are found close to a 2D disordered hexagonal packing thanks to a fit of the data with the software FitGISAXS (fitting procedure is described in Supp. Info.). The conservation of these orders through the whole film thickness confirms the perpendicular orientation of the cylinders all over the thickness.

The agreement between AFM and GISAXS experiments is of importance since the sample areas studied by these two methods are quite different in size. While the GISAXS experiments investigate the whole sample (1 cm^2), the AFM method focuses on the local organization (1 µm^2). The GISAXS $I(Q_y)$ presents a limited number of peaks with significant width (four orders). This suggests a limited range of the hexagonal correlation. It is in agreement with the presence of packing defects in the AFM images (e.g. Figure 1.a). Nevertheless, this local organization is confirmed by the fit of the GISAXS data to persist through the whole film thickness.

Films (thickness 80 nm) of PS-b-P2VP organized in parallel cylinders were also prepared, by spin-coating a PS_{34}-b-$P2VP_{18}$ solution in chloroform. A further annealing in chloroform vapors for 1 min was found essential to obtain the parallel orientation of the cylinders.

Formation of plasmonic gold nanoparticles by sonication.

The incorporation of the inorganic gold salt into one of the copolymer domains is one possible way to achieve the single-step synthesis of AuNPs organized in a copolymer film[44]. Generally, the reduction step is obtained *via* a chemical reducing agent, or UV or heat exposure.

Here addition of a gold salt ($AuCl_3$) in the PS_{27}-b-$P4VP_7$ copolymer solution and further sonication leads to the formation of AuNPs. The formation of AuNPs over time was demonstrated by UV-visible spectroscopy, evidencing the decrease of the Au(III) peak at 325 nm (Figure 3.a). Au(III) has signatures in UV-visible in the 200-350 nm range depending on the nature of the ligand and solvent[45]. The optimal sonication time was found to be 6 min at this concentration, since for

Published on 10 July 2018. Downloaded on 7/16/2018 5:59:18 AM.

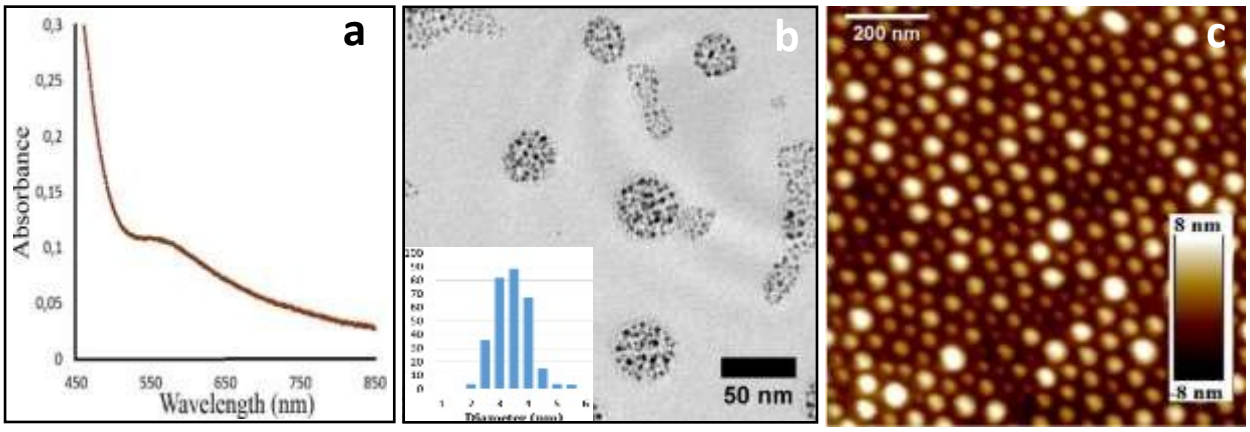

Figure 5. a/ UV-visible spectra (minus the copolymer contribution) showing the plasmon resonance of the AuNPs after their growth; b/ TEM picture of the bigger AuNPs (3-4 nm) confined in the PVP domain of PS27-b-P4VP7, formed by seeded-growth with sonication, with inset the size distribution of the AuNP diameter. The average NP diameter is 3.5 nm; c/AFM height picture of a film obtained by spin-coating the same solution on a wafer. If the 2D-hexagonal organization seems unaffected by the presence of the AuNPs, a disparity in the diameters of the cylinders can be noticed as well as an increase of the mean diameter when compared to the films without AuNPs.

longer times an increase of the Au(III) signal is observed, indicating the re-oxidation of a gold species into Au(III). This phenomenon could be attributed to an effect of oxidizing agents formed by the sonication process, but this point was not further studied. TEM pictures (Figure 3.b) of a drop-cast film from the solution shows the AuNPs formed by sonication, confined inside the P4VP domains, due to the affinity between gold and the pyridine group of P4VP[46]. TEM analysis realized by drop-casting the copolymer solution, with or without nanoparticles, on a TEM carbonated-grid shows an organized microphase-separated film, although it is known that such procedure can produce different morphologies than spin-coating. However this perfectly discriminates the preferential location of nanoparticles between PS and PVP domains.The average NP diameter determined by image analysis on the TEM micrographs (inset in Figure 3.c) was found to be 2-3 nm. This size is not large enough to provide the AuNPs with suitable plasmonic properties and, thus, explains the absence of a plasmon peak in the UV-visible spectra.

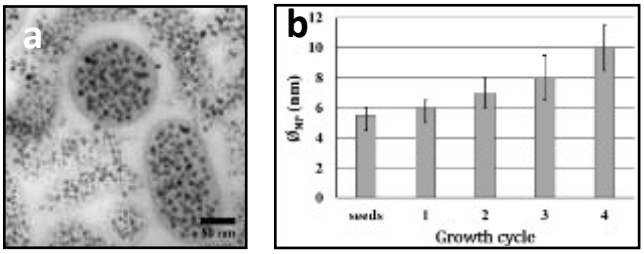

Figure 6. a/ TEM picture of the PVP domain of PS48-b-P4VP25 containing AuNPs pre-formed by sonication for an initial ratio Au/pyr = 3.5 after a seeded-growth process (growth cycles adding a ratio Au/pyr = 0.2 each time) with 3 growth cycles, with inset the size distribution of the AuNP diameter over 100 AuNPs, and b/ evolution of the nanoparticle diameter with the number of growth cycles carried out.

A study of the initial amount of gold in solution was performed, with the preparation of copolymer solutions containing gold salt, with a ratio Au/pyr from 0.1 to 5.5. Figure 4 and Supp. Info. S5 show the TEM pictures of the films produced with these increasing concentrations: while the AuNPs are barely visible for a ratio Au/pyr = 0.2 and not visible at all for 0.1, not shown, they become quite visible beyond a ratio of 0.5. With increasing the ratio gold/pyridine, the AuNPs produced by sonication are larger. From 2 nm for Au/pyr = 0.5, a diameter of 3.5 nm was reached when increasing the ratio to 5.5.

Another way to get larger nanoparticles is through a seeded-growth process over a solution of AuNPs formed by sonication in the copolymer, with an initial ratio gold/pyridine = 0.5. After the first reduction by sonication, a second amount of gold salt (Au/pyr = 0.2) was added in the solution AuNPs/copolymer, and sonicated. The process was repeated again (up to four times) to obtain AuNPs large enough to exhibit plasmonic properties: indeed, a small bump is visible at a wavelength of 560 nm in the UV-visible spectroscopy data obtained for the AuNPs/copolymer suspension (Figure 5.a). This bump can be attributed to a plasmon resonance damped by small-size effects[47]. TEM picture of the film formed with such a solution shows larger AuNPs inside the P4VP domains (Figure 5.b). The average diameter of these AuNPs is 3-4 nm. This seeded-growth process was found interesting for it used a total ratio Au/pyr of 1 in order to reach the same sizes of particles as the solution with an initial ratio Au/pyr = 3.5. We can propose that this difference between the two processes is due to a favorized growth over the nucleation in the case of the seeded-growth process. This seeded-growth process was performed over a solution containing AuNPs with a larger diameter of 5.5 nm with cycles of addition/reduction adding a ratio Au/pyr = 0.2 each time and led to the formation of films containing bigger AuNPs, with a diameter up to 10 nm, located preferentially in the PVP domains (Figure 6).

Published on 10 July 2018. Downloaded on 7/16/2018 5:59:18 AM.

Impact of the AuNPs over the cylinders organization.

The incorporation of AuNPs inside PS_{34}-b-$P2VP_{18}$ copolymer film was found to prevent their parallel organization. Studies have already demonstrated the use of functionalized NPs to direct the orientation of block copolymers[48,49]. Here, we have observed the absence of the parallel orientation of cylinders after the *in situ* formation of AuNPs by sonication of the copolymer/Au salt solution. Figures 7.a and 7.b show the AFM height pictures of PS-b-P2VP films after solvent annealing without and with AuNPs. The film spin-cast with AuNPs formed by sonication present a disorganization of the cylinders. This is linked to the presence of the AuNPs in the solution, since the same sample in absence of AuNPs and subject to sonication for 6 min prior to spin-coating produces identical pattern of parallel cylinders.

No effect of AuNPs was detected on the perpendicular orientation of the PS_{27}-b-$P4VP_7$ cylinders, as we can see in Figures 3 and 5. The conservation of the perpendicular orientation when AuNPs are included in PS_{27}-b-$P4VP_7$ films is confirmed by the GISAXS experiments, with the appropriate fit of data (Figure 8; Table 3), which demonstrate the same 2D-hexagonal organization in surface compared to the same film without gold.

Angle (mrad)	D (nm)	Λ (nm)	H (nm)	σ (nm)
2	**26.2**	**26.7**	80.7	21.8
2.5	**25.0**	**29.0**	77.7	20.0
3	**26.0**	**29.7**	81.0	15.0
3.5	**26.0**	**28.6**	80.1	18.0
4	**26.0**	**27.3**	80.1	22.0
AFM	**26.0**	**41.9**	80.0	//

Table 3. Parameters of 2D-fit for every incidence angle, with 2D-hexagonal local monodisperse approximation, in comparison with AFM measurements for a PS27-b-P4Vp7 film containing AuNPs formed by sonication (AuNP diameter = 2 nm). σ is the standard deviation from the cylinder diameter.

The second peak is almost invisible, which means a 2D-hexagonal organization on a less-extended range than for the samples without AuNPs (see Supp. Info.; S6). It can be noticed that in the case of the sample with AuNPs, the first order peak is more pronounced at 3 and 3.5 mrad. If the AuNPs are responsible to the slight disorganization of the cylinder orientation, it may indicate that they are mostly localized at the interfaces air/film and film/substrate, since the disorganization is stronger for these positions (corresponding to 2 and 4 mrad, respectively). Actually, this localization is supported by preliminary tomography experiments (to be published). The FitGISAXS analysis (example of the fit curve for 4 mrad is shown in the Figure 8.b) allows a determination of

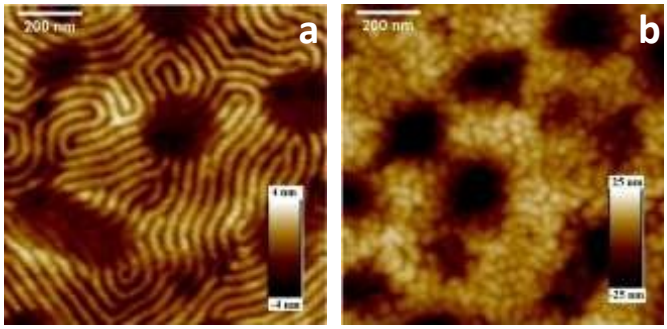

Figure 7. AFM height pictures of the cylinders of PS34-b-P2VP18 a/ without, and b/ with AuNPs formed by sonication (Au/pyr = 0.5). The presence of AuNPs triggers the re-orientation of the cylinders. Scale bar is 200 nm.

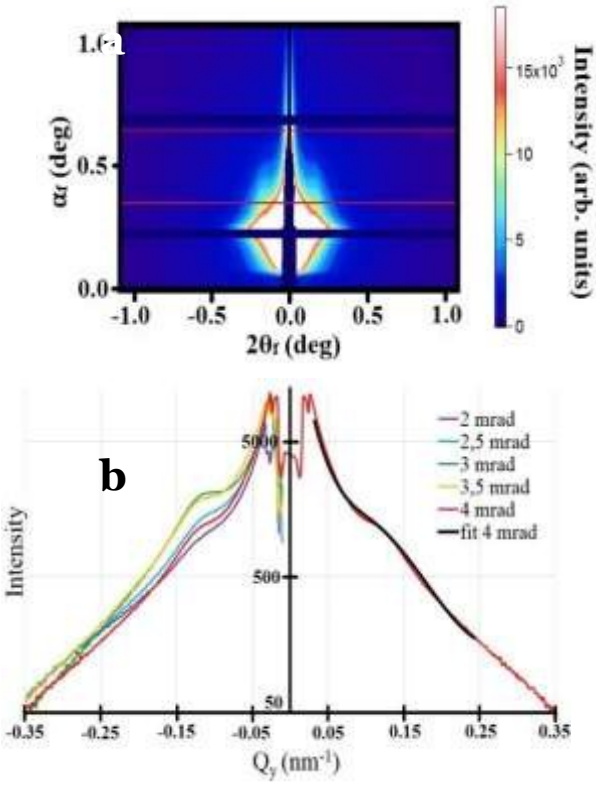

Figure 8. a/ GISAXS pattern for a PS27-b-P4VP7 film containing the AuNPs formed by sonication (AuNP diameter = 2 nm), for an incidence angle of 3 mrad, and the corresponding intensity versus Qy curve (integrated between the two red lines of a)) with b/ intensity versus Qy curves for all the incidence angle analyzed. A slight modification of the organization is seen for the incidence angle of 4 mrad. The fit of the data (see details in text) for 4 mrad is shown (black curve).

the structural parameters (diameter of the cylinders (D), center-to-center distance (Λ), and thickness of the film (H), as well as the standard deviation (σ)) for the films containing AuNPs for all incidence angles (Table 3). These results deduced

from the fit are in accordance with the AFM pictures concerning the diameter and the thickness of the sample, which do not change in the case of films containing small AuNPs (diameter 2 nm) from the gold-free films.

In the case of the film containing the AuNPs formed by seeded-growth method, AFM measurements (Figure 9) show an increase in the mean diameter of the cylinders: from a mean diameter of 32 nm without the AuNPs the cylinders containing AuNPs reach diameters up to 62 nm over the reduction cycles. This result confirms the presence of the AuNPs inside the PVP domains and quantifies the alteration such particles operate on the film morphology.

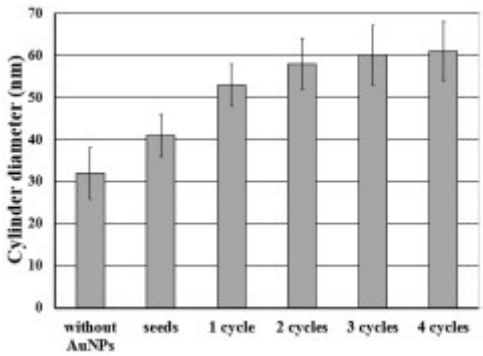

Figure 9. Average diameter of the PS48-b-P4VP25 cylinders upon the growth cycles forming the AuNPs, over 100 cylinders. The PVP domains swell in presence and with the size of the AuNPs, as shown by the increasing of the cylinder diameter.

Formation of AuNPs by radiolysis.

Another approach to the *in situ* formation of AuNPs in an organized copolymer film was to use radiolysis. Interestingly, the irradiation of either a gold containing-copolymer solution or of the spin-cast film obtained with this solution equally shows the formation of AuNPs. Mößmer *et al.*[50] have shown that after incorporation of a gold salt in PS-b-P2VP micelles, the electron beam of the microscope can reduce the gold salt into small NPs located in the PVP core of the micelles. A similar case of palladium nanoparticles formation in organic media (toluene) has been studied by Abellan *et al.*[51] and gives clues about the mechanism involved in such a reaction.

In our case, after 24h of irradiation of a mixture of $AuCl_3$ gold salt and PS_{27}-b-$P4VP_7$ copolymer in toluene/THF solution, UV-visible spectroscopy (Figure 10.a) shows a plasmon resonance at λ~565 nm, confirming the formation of AuNPs. The same plasmon peak appears in transmission for the irradiated film after 3 hours of irradiation and is still present after 24 hours (data not shown). The dose of irradiation is of 1 kGy after 3 hours, which is a weak dose[52]. This could confirm a catalytic effect of the first AuNPs formed in solution which would enhance the reduction of gold on their surface and promote the AuNP growth. TEM micrographs (Figure 10.b) for the irradiated solution show the AuNPs inside the cylinders of the copolymer. The average diameter of these nanoparticles is around 3.5 nm, which is enough to observe a damped plasmon resonance. Unlike the spin-coating, the deposition on the TEM grid, by drop-casting, allows microphase separation of the diblock structures, but does not produce any 2D-organization. For the spin-cast gold-containing film after irradiation, the 2D organization is conserved at least on the surface, as shown in AFM images as Figure 10.c.

Optical responses.

We studied by variable angle spectroscopic ellipsometry (VASE) the films with different growth steps of the gold nanoparticles by sonication. The information contained in the ellipsometry data can be represented as the (Ψ, Δ) angle pair or the complex numbers $\rho=r_p/r_s=\tan(\Psi).e^{i\Delta}$, or $\tilde{\varepsilon}=\tilde{\varepsilon}_r+i.\tilde{\varepsilon}_i=\sin^2(\theta_0)\left[1+\left(\frac{1-\rho}{1+\rho}\right)^2\tan^2(\theta_0)\right]$, (see Experimental section). The Figure

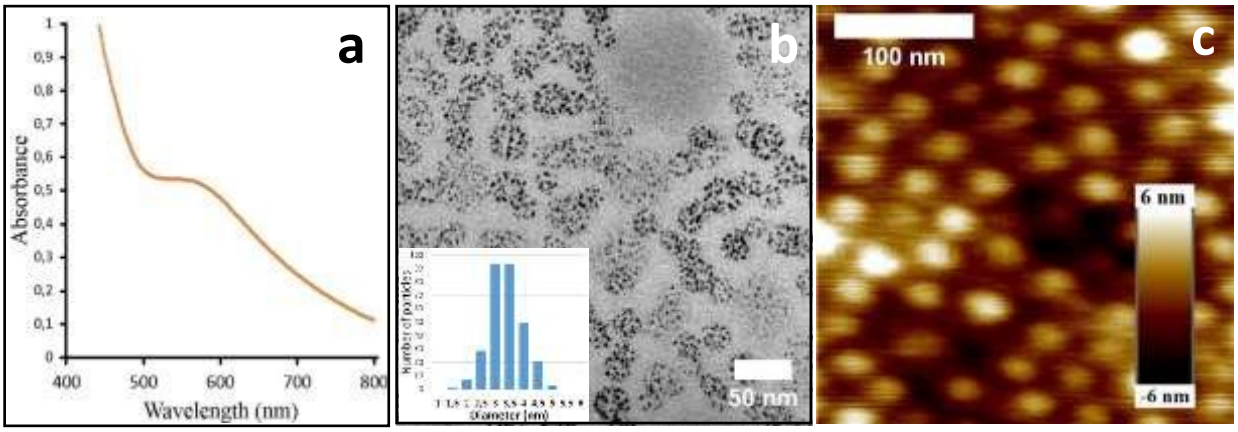

Figure 10. a/ UV-visible spectrum (minus the copolymer contribution) showing the plasmon resonance of the AuNPs containing-solution after 24 h of irradiation; b/ TEM picture of the same sample after deposition on a TEM grid, showing the AuNPs confined in the cylinders of PS27-b-P4VP7, with inset the size distribution of the AuNPs diameter over 300 particles. The average diameter of 3.5 nm is responsible for the plasmonic properties exhibited by the AuNPs; and c/ AFM height picture of the gold containing-film after radiolysis showing that the orientation of the cylinders is still normal to the substrate and the 2D organization is conserved.

Published on 10 July 2018. Downloaded on 7/16/2018 5:59:18 AM.

Published on 10 July 2018. Downloaded on 7/16/2018 5:59:18 AM.

11.a shows the real part of $\tilde{\varepsilon}$ as a function of the photon energy between 0.6 and 4.5eV, for the films with different AuNPs sizes (described in Figure 6.b). The signal from the seed-loaded film, also reproduced in the inset for clarity, shows regular oscillations related to the interferences driven by reflections at the air/film and film/substrate interfaces, showing that the film is mostly transparent in the studied energy range. The Au seeds are too small to produce a strong plasmon resonance, and the UV absorption bands of the possibly remaining $AuCl_3$ salt or the solid seeds are weak enough. As the AuNPs are grown with successive cycles, we observe that the oscillations of the curve are damped and shifted to higher energies. Since the films all have similar thicknesses, we can relate these evolutions to both an increase of the films absorption, and a change in their effective refractive index. These changes can be associated to the increase of the gold volume fraction and the appearance of a plasmon absorption band when the AuNPs grow.

Extracting the optical index or the dielectric function of a thin film of material deposited on a substrate, from the ellipsometric data, requires an appropriate optical model of the permittivity of the film, which can be challenging for nanostructured and anisotropic materials such as the ones studied here. For simple composites of plasmonic NPs, it is usual to build the optical model with a combination of a few Lorentz oscillators, but no such simple combination could be fitted to our measurements, although the response of the studied thin films with large enough particles (> 4 nm) most likely contains plasmonic resonances.

The ellipsometric data of the films, however, show the existence of a cancellation of the ellipsometric intensity angle Ψ, while the ellipsometric phase angle Δ jumps abruptly of more than 180° at a given incidence angle and photon energy. In the example shown on the Figure 11.b, for the film with the AuNPS obtained by two growth cycles (AuNPs diameter of 7 nm), this specific behavior occurs at an incident light energy of 2.55 eV and incidence angle of Θ_o = 65°.

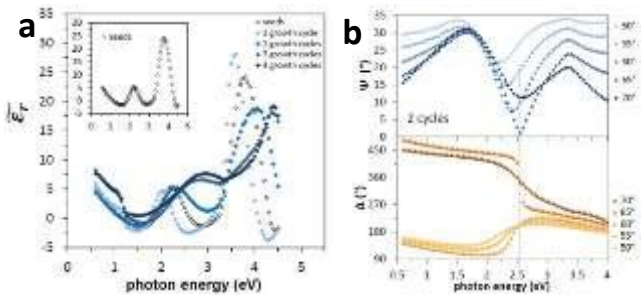

Figure 11. a/ Ellipsometry data plotted as the real part of $\tilde{\varepsilon}$ as a function of the photon energy for films including AuNPs formed by the seeded-growth method with different numbers of growth cycles; the curve for the film including seeds is repeated in inset for clarity; b/ ellipsometric angles (Ψ, Δ) as a function of the photon energy for different angles of incidence Θo from 50 to 70° for the film including AuNPs formed by two growth cycles. An annulation of Ψ and a jump in Δ are visible for an energy of 2.55eV (λ=486nm) and an angle of incidence of Θo=65°.

This behavior has been called "plasmon-induced Brewster" extinction[12] or "topological darkness" because the exact cancellation of the ellipsometric parameter ρ, or equivalently of the ellipsometric angle Ψ, is guaranteed geometrically by the Jordan theorem[53]. It has been identified as a method to reach highly sensitive plasmonic detection[53] in biological or chemical sensors, thanks to the very large phase jump. The dark point returned by the ellipsometer as Ψ = 0, simply corresponds to the conditions for which the p-polarized light is not reflected (r_p = 0). For a simple isotropic film, which can be described by a single effective optical index N=n+ik, this extinction corresponds to a specific combination of the parameters defining r_p, through the Fresnel coefficients, namely the wavelength λ, the angle of incidence Θ_o, the index N=n+ik of the film material and those of the ambient (air) and substrate media. For anisotropic plasmonic material, it has been shown that the dark point can still be predicted by simulations if a reliable structural model of the thin film is known[12].

Note that in the previous evidences of topological darkness in nanoplasmonic systems[12,53,54,55], the studied thin films presented pronounced plasmon resonances responsible for strong light absorption. On the opposite, all the samples of the studied series, from the seed-loaded film to the films including post-grown AuNPs, present the darkness feature regardless of pronounced plasmon resonance, therefore providing possible materials for low-loss sensitive detection devices. For all these films of same surrounding and very similar thicknesses, the dark points occur at very close angles of incidence (all within a few degrees around 65°) and energies increasing with the size of the AuNPs: 2.3 eV, 2.25 eV, 2.55 eV, 2.7 eV and 3.1 eV for the films with Au-seeds, and with AuNPs from 1, 2, 3 and 4 growth cycles, respectively. The energy shifts are additional evidences of the effect of the NP-growth on the optical responses of the host films. The supplementary information file displays the comparison of the Ψ and Δ curves for the 2 and 3-cycle samples as an example (Figure S7 in the SI).

Conclusions

We produced anisotropic films of block copolymer PS-b-PVP containing *in situ* synthetized AuNPs of controlled sizes between 2 nm and 4 nm aligned along oriented cylinders. Well-ordered structures of perpendicular and parallel PVP cylinders embedded in the PS matrix were prepared, thanks to the appropriate solvent deposition and solvent annealing. The perpendicular cylinder morphology spans over the film thickness as demonstrated by GISAXS, even when AuNPs are present in the PVP cylinders.

AuNPs were formed from physically-activated reduction (by sonication or irradiation) of the gold salt mixed with the copolymer solution, prior to their casting as films.

The sonication of a mixture of gold salt/copolymer leads to the formation of AuNPs of small size (< 2 nm), confined in the PVP block domains (*i.e* the cylinders) after the film deposition.

AuNPs formed by sonication were found to induce no significant deformation of the structure for perpendicular cylinders, while they affect the organization of the parallel cylinders, redirecting them to a quasi-perpendicular orientation. Bigger size (~ 4 nm) AuNPs with plasmon resonance properties could also be obtained, either by increasing the initial gold quantity in the mixture, or by a seeded-growth method of the already formed AuNPs. In the latter case, the plasmonic particles formation was more efficient for less initial gold precursor. For these bigger sizes, conservation of the 2D-hexagonal organization of the cylinders was observed, but with some modifications in the size of the cylinder diameters.

γ-ray irradiation of the gold salt/copolymer solution was demonstrated as an alternative method to lead to similar AuNPs. We have also shown that the γ-ray irradiation of the film of a spin-cast gold salt/copolymer mixed solution leads to *in situ* formation of plasmonic AuNPs in the perpendicular cylinders of the copolymer. This alternative allows the formation of the AuNPs in a film already deposited without altering its morphology. Such simple methods for the formation of plasmonic AuNPs, paired with their selective location in a self-assembled copolymer film will be of great interest as a new bottom-up process for the formation of nanoplasmonic materials and metamaterials.

These methods also offer a very controlled way for easily inserting dense population of small size AuNPs (< 2 nm) in an organic nanostructured film.

Finally, we demonstrate promising optical properties for these hybrid films with an extinction accompanied by a phase jump at specific wavelength and incidence angle. The dependence on the wavelength and angle with the nanoparticle size is the first step towards modulation of optical properties for the bottom-up formation of hybrid nanostructures.

Conflicts of interest

There are no conflicts to declare.

Acknowledgements

We are very thankful for the help of Pierre-Eugène COULON (Laboratoire des Solides irradiés, Ecole Polytechnique; FRANCE) in the TEM characterization of our materials. The participation of Jean-Philippe RENAULT (Laboratoire Interdisciplinaire à l'Organisation Nanométrique et Supramoléculaire, CEA-Saclay; France) for the radiolysis part is also warmly acknowledged.

Allocation of beamtime on the beamline SIRIUS of the French synchrotron SOLEIL is gratefully acknowledged.

This work was supported by the Conseil Régional d'Aquitaine. It has benefited from the support of the LabEx AMADEus (ANR-10-LABX-42) in the framework of IdEx Bordeaux (ANR-10-IDEX-03-02), France.

Notes and references

1 M.-C. Daniel and D. Astruc, *Chem. Rev.* 2004, **104**, 293.
2 A. Boymelgreen, G. Yossifon and T. Miloh, *Langmuir* 2016, **32**, 9540
3 W. L. Barnes, A. Dereux, T. W. Ebbesen, *Nature* 2003, **424**, 824
4 K. L. Kelly, E. Coronado, L. L. Zhao, G. C. Schatz, *J. Phys. Chem. B* 2003, **107**, 668
5 F. S. Bates, G. H. Fredrickson, *Phys. Today* 1999, **52**, 32
6 H.-C. Kim, D. Hinsberg, *J. Vac. Sci. Technol.* 2008, **26**, 1369
7 I. W. Hamley, *Progress in Polymer Science* 2009, **34**, 1161
8 S. B. Darling, *Progress in Polymer Science* 2007, **32**, 1152
9 S. Vignolini, N. A. Yufa, P. S. Cunha, S. Guldin, I. Rushkin, M. Stefik, K. Hur, U. Wiesner, J. J. Baumberg, U. Steiner, *Adv. Mater.* 2012, **24**, OP23
10 S. Salvatore, A. Demetriadou, S. Vignolini, S. S. Oh, S. Wuestner, N. A. Yufa, M. Stefik, U. Wiesner, J. J. Baumberg, O. Hess, U. Steiner, *Adv. Mater.* 2013, **25**, 2713
11 X. Wang, K. Ehrhardt, C. Tallet, M. Warenghem, A. Baron, A. Aradian, M. Kildemo, V. Ponsinet, *J. Opt. & Laser Techn.* 2017, **88**, 85
12 J. Toudert, X. Wang, C. Tallet, P. Barois, A. Aradian, V. Ponsinet, *ACS Photonics* 2015, **2**, 1443
13 J. A. Schuller, E. S. Barnard, W. Cai, Y. C. Jun, J. S. White, M. L. Brongersma, *Nat. Mat.* 2010, **9**, 193
14 J. J Armao, Y. Domoto, T. Umehara, M. Maaloum, C. Contal, G. Fuks, E. Moulin, G. Decher, N. Javahiraly, N. Giuseppone, *ACSNano* 2016, **10**, 2082
15 C. T. Black, R. Ruiz, G. Breyta, J. Y. Cheng, M. E. Colbum, K. W. Guarini, H.-C. Kim, Y. Zhang, *J. Res. & Dev.* 2007, **51**, 605
16 L. Ferrari, C. Wu, D. Lepage, X. Zhang, Z. Liu, *Progress in Quantum Electronics* 2015, **40**, 1
17 K. V. Sreekanth, Y. Alapan, M. ElKabbash, E. Ilker, M. Hinczewski, U. A. Gurkan, A. De Luca, G. Strangi, *Nat. Mat.* 2016, **15**, 621
18 R. E. Cohen, *Solid. State Mater. Sci.* 1999, **4**, 587
19 B. H. Sohn, B. H. Seo, *Chem. Mater.* 2001, **13**, 1752
20 S. Kim, G. Jeon, S. W. Heo, H. J. Kim, S. B. Kim, T. Chang, J. K. Kim, *Soft Matter* 2013, **9**, 5550
21 B. Rasin, H. Chao, G. Jiang, D. Wang, R. A. Riggleman, R. J. Composto, *Soft Matter* 2016, **12**, 2177
22 E B. Gowd, B. Nandan, N. C. Bigall, A. Eychmüller, P. Formanek, M. Stamm, *Polymer* 2010**, 51**, 2661
23 H. Cho, H. Park, T. P. Russell, S. Park, *J. Mater. Chem.* 2010, **20**, 5047
24 M. Aizawa, J. M. Buriak, *Chem. Mater.* 2007, **19**, 5090
25 D. O. Shin, D. H. Lee, H.-S. Moon, S.-J. Jeong, J. Y. Kim, J. H. Mun, H. Cho, S. Park, S. O. Kim, *Adv. Funct. Mater.* 2011, **21**, 250
26 K. Aissou, M. Mumtaz, A. Alvarez-Fernandez, J. Mercat, S. Antoine, G. Pécastaings, V. Ponsinet, C. Dobrzynski, G. Fleury, G. Hadziioannou, *Macromol. Rapid Commun.* 2018, 1700754
27 J. Zhao, X. C. Chen, P. F. Green, *Soft Matter* 2013, **9**, 6128
28 C.-M. Chen, Y.-J. Huang, K.-H. Wei, *Nanoscale* 2014, **6**, 5999
29 S. G. Jang, A. Khan, C. J. Hawker, E. J. Kramer, *Macromolecules* 2012, **45**, 1553
30 R. D. Deshmukh, Y. Liu, R. J. Composto, *Nano Letters* 2007, **7**, 3662
31 P. A. Mistark, S. Park, S. E. Yalcin, D. H. Lee, O. Yavuzcetin, M. T. Tuominen, T. P. Russell, M. Achermann, *ACSNano* 2009, **3**, 3987
32 M. R. Bockstaller, R. A. Mickiewicz, E. L. Thomas, *Adv. Mater.* 2005, **17**, 1331
33 Wang, F. Montagne, P. Hoffmann, H. Heinzelmann, R. Pugin, *J. Coll. Inter. Science* 2011, **356**, 496

Published on 10 July 2018. Downloaded on 7/16/2018 5:59:18 AM.

34 W. Abidi, P. R. Selvakannan, Y. Guillet, I. Lampre, P. Beaunier, B. Pansu, B. Palpant, H. Remita, *J. Phys. Chem. C* 2010, **114**, 14794
35 W. Abidi, B. Pansu, R. Krishnaswamy, P. Beaunier, H. Remita, M. Imperor-Clerc, *RSC Advances* 2011, **1**, 434
36 E. Gachard, H. Remita, J. Khatouri, B. Keita, L. Nadjo, J. Belloni, *New Journal of Chemistry* 1998, **22**, 1257
37 A. L. González-Mendoza, L. I. Cabrera-Lara, *J. Mex. Chem. Soc.* 2015, **59**, 119
38 K. Okitsu, M. Ashokkumar, F. Grieser, *J. Phys. Chem. B* 2005, **109**, 20673
39 J. K.-J. Li, C.-J. Ke, C.-A. Lin, Z.-H. Cai, C.-Y. Chen, W. H. Chang, *J. Med. Biolog. Engineer.* 2011, **33**, 23
40 G. Surendran, M. S. Tokumoto, E. Pena dos Santos, Remita, H.; L. Ramos, J. Kooyman, C. V. Santilli, C. Bourgaux, P. Dieudonné, E. Prouzet, *Chem. Mater* 2005, **17**, 1505
41 P. Fontaine, G. Ciatto, N. Aubert, M. Goldmann, *Sci. Adv. Mater.* 2014, **6**, 2312
42 D. Babonneau, *J. Appl. Crystallog.* 2010, **43**, 929
43 S. Park, J.-Y. Wang, B. Kim, W. Chen, T. P. Russell, *Macromolecules* 2007, **40**, 9059
44 J. P. Spatz, S. Mössmer, M. Möller, *Chem. Eur.* 1996, **12**, 1552
45 M. J. Liew, S. Sobri, S. Roy, *Electrochimica Acta* 2005, **51**, 877
46 J. Q. Lu, S. S. Yi, *Langmuir* 2006, **22**, 3951
47 J. Vieaud, O. Merchiers, M. Rajaoarivelo, M. Warenghem, Y. Borensztein, V. Ponsinet, A. Aradian, *Thin Solid Films* 2016, **603**, 452
48 B. J. Kim, J. J. Chiu, G.-R. Yi, D. J. Pine, E. J. Kramer, *Adv. Mater.* 2005, **17**, 2618
49 S. Kim, H. S. Wang, S. G. Jang, S.-H. Choi, B. J. Kim, J. Bang, *J. Polym. Sci., Part B: Polymer Physics* 2016, **54**, 118
50 S. Mössmer, J. P. Spatz, M. Möller, *Macromolecules* 2000, **33**, 4791
51 P. Abellan, L. R. Parent, N. Al Hasan, C. Park, I. Arslan, A. M. Karim, J. E. Evans, N. D. Browning, *Langmuir* 2016, **32**, 1468
52 H. Remita, I. Lampre, M. Mostafavi, E. Balanzat, S. Bouffard, *Radiation Physics and Chemistry* 2005, **75**, 575
53 V. G. Kravets, F. Schedin, R. Jalil, L. Britnell, R. V. Gorbachev, D. Ansell, B. Thackray, K. S. Novoselov, A. K. Geim, A. V. Kabashin, A. N. Grigorenko, *Nat. Mater.* 2013, **12**, 304
54 L. Malassis, P. Massé, M. Tréguer-Delapierre, S. Mornet, P. Weisbecker, P. Barois, C. R. Simovski, V. G. Kravets, A. N. Grigorenko, *Adv. Mater.* 2014, **26**, 324
55 B. Vasic, R. Gajic, *J. Appl. Phys*. 2014, **116**, 023102

Published on 10 July 2018. Downloaded on 7/16/2018 5:59:18 AM.